

Entanglement renormalization in free bosonic systems: real-space versus momentum-space renormalization group transforms

G. Evenbly¹ and G. Vidal¹

¹*School of Physical Sciences, the University of Queensland, QLD 4072, Australia*

(Dated: February 6, 2020)

The ability of entanglement renormalization (ER) to generate a proper real-space renormalization group (RG) flow in harmonic lattice systems of $D = 1$ and $D = 2$ spatial dimensions is analyzed. A conceptual overview of the steps involved in momentum-space RG is provided and contrasted against the equivalent steps in the real-space setting. The real-space RG flow, as generated by ER, is compared with exact results from momentum space including an investigation of a critical fixed points and examples with relevant/irrelevant perturbations.

PACS numbers:

I. INTRODUCTION

The renormalization group (RG) is a set of tools and ideas used to investigate how the physics of an extended system changes with the scale of observation [1, 2, 3, 4, 5, 6, 7]. The RG plays a prominent role in the conceptual foundation of several areas of physics concerned with systems that consists of many interacting degrees of freedom, as is the case of quantum field theory, statistical mechanics and condensed matter theory [1, 2, 3, 4, 5]. In addition it also provides the basis for important numerical approaches to study such systems [5, 6, 7].

Given a microscopic description of an extended system in terms of its basic degrees of freedom and their interactions, RG methods aim to obtain an *effective theory*, one that retains only some of these degrees of freedom but is nevertheless still able to reproduce its low energy (or long distance) physics. The effective theory is obtained through coarse-graining transformations that remove those degrees of freedom deemed to be *frozen* at the observation scale of interest. Broadly speaking, RG techniques fall into two categories depending on how the coarse-graining is implemented, namely momentum-space RG [3] and real-space RG [6, 7].

Momentum-space RG is applied to theories that are expressed in fourier space. It works by integrating out high-momentum modes of a field and it is often associated to perturbative approaches [3]. Instead, real-space RG is applied directly to theories that are written in terms of local degrees of freedom, say spins in the case of a spin system defined on a lattice. It is not linked perturbation theory and can in particular be applied to strongly interacting systems. As proposed by Kadanov [4], the coarse-graining transformation is implemented by replacing a block of spins with a single effective spin, a procedure refined by Wilson [5] and subsequently turned by White into the density matrix renormalization group (DMRG) algorithm [6, 7], an impressively precise numerical tool to study one-dimensional systems.

A major difficulty of momentum-space RG comes precisely from the fact that it requires, as a starting point,

a description of the system in fourier space. Such description is not always available and might not be obtained easily. Consider for instance a system of interacting spins, as specified by some generic spin-spin interaction. There obtaining a momentum space representation might be as difficult as solving the whole theory. In this and many other cases, a RG approach must be performed in real space.

In spite of its indisputable success, the DMRG algorithm —by far the best available real-space RG approach to quantum systems on a lattice— suffers from a shortcoming that has important implications. Because of the accumulation of short-ranged entanglement near the boundary of a spin block, the dimension of the Hilbert space used to effectively describe the block must grow with each iteration of the RG transformation. As a result, for instance, fixed points of the RG flow (scale invariant critical systems) cannot be fixed points of the DMRG algorithm. Another, more practical consequence of this growth is that it limits the size of $1D$ critical systems that can be analyzed and, most importantly, it severely limits the success of DMRG computations in higher spatial dimensions.

Entanglement renormalization (ER) is a real-space RG method recently proposed in order to overcome the above difficulties [8]. The main feature of ER is the use of *disentangler*s. These are unitary transformations, locally applied near the boundary of a spin block, that remove short-ranged entanglement before the system is coarse-grained. As a result, the effective dimension of the Hilbert space for a spin block can be kept constant under successive RG transformations, so that the approach can be applied to arbitrarily large systems. The potential of ER —as well as that of the related variational ansatz, the *multi-scale entanglement renormalization ansatz* (MERA) [9]— to efficiently describe critical and non-critical ground states has already been demonstrated for a number of spin and free fermions models in one [8] and two spatial dimensions [10, 14]. In addition, it has been shown that the MERA offers a natural representation for systems with topological order. Finally, several algorithms to compute the MERA have been put

forward [11, 12, 13].

In this work we explore the performance of an ER-based real-space RG transform in a system of free bosons. Our goal is to test the ability of ER to produce a sensible RG flow, one with the expected structure of fixed points and flow directions according to relevant and irrelevant Hamiltonian terms. For this purpose, we consider discretized versions of real free Klein-Gordon field theories, which correspond to harmonic lattice systems. Such systems are an ideal testing-ground for ER. On the one hand, they can be fully characterized in terms of correlation matrices, fact that simplifies the analysis and conveniently reduces the computational complexity of MERA calculations. On the other hand, an RG analysis of free-particle theories can be conducted simply and without approximations in momentum space. This allows for a comparison between the numerical results obtained using ER and the exact solution.

Specifically, we show that a ER-based real-space RG transform is able to reproduce the exact results from momentum space RG to a high accuracy in $D = 1, 2$ dimensional infinite lattice systems, both for the critical and non-critical cases considered. We also demonstrate the ability of the MERA to provide an efficient and accurate representation of ground-state of free boson systems, thus extending to the bosonic case the results of [10]. It is expected that the ER approach, which can be implemented without making use of the special properties of free-particle systems [11, 12, 13], will perform in a similar way in strongly interacting systems not tractable with momentum-space RG approaches.

An overview of this work is presented schematically in Fig. (1); equivalently the paper is organized as follows. Sec. II introduces the harmonic system under consideration. In Sec. III the process of renormalizing the system in momentum-space is explained, highlighting conceptual features of the RG. The critical system, and examples of relevant and irrelevant perturbations to critical case are considered. Sec. IV explains the details of performing real-space RG with ER numerically, both in terms of renormalizing Hamiltonians and ground-states. In Sec. V results are presented, including comparisons between the exact and the numerical calculations. Appendix A provides details on the variational approach used to find the disentangles for the ER method. Appendix B provides details for the derivation of the ground-state covariance matrices, including a prescription for how the critical case may be regularized.

II. COUPLED HARMONIC OSCILLATORS

We consider cubic harmonic lattices in $D = 1$ and $D = 2$ spatial dimensions. For clarity the present derivation is continued the present in terms the $1D$ setting; the generalization of these workings to the $2D$ systems follows easily. The Hamiltonian for a chain of N harmonic oscillators each with mass m , angular frequency ω , and

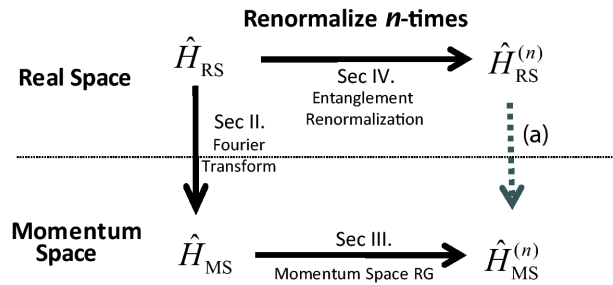


FIG. 1: A conceptual outline of this paper. The system Hamiltonian \hat{H}_{RS} , defined in terms of interaction between local degrees of freedom, may be renormalized directly with a numeric implementation of real-space RG, such as entanglement renormalization (ER), as outlined in Sec. IV. Iterating the RG n times we get the n^{th} renormalized Hamiltonian $\hat{H}_{RS}^{(n)}$. The system may also be renormalized by first transforming the Hamiltonian to a momentum-space representation \hat{H}_{MS} , via fourier transform of the canonical coordinates, as described in Sec. II. Momentum-space RG may be applied (analytically) to \hat{H}_{MS} ; this is described Sec. III. In order to compare the results of the two methods, the real-space Hamiltonians, $\hat{H}_{RS}^{(n)}$, are diagonalized (step (a)), and the dispersion relations compared to those of the corresponding momentum-space Hamiltonians, $\hat{H}_{MS}^{(n)}$.

coupled via nearest neighbour with a ‘spring constant’ K , is written

$$\begin{aligned} \hat{H} &= c_0 \sum_{r=1}^N \left(\frac{1}{2m} \hat{p}_r^2 + \frac{m\omega^2}{2} \hat{q}_r^2 + K (\hat{q}_{r+1} - \hat{q}_r)^2 \right) \\ &= \sum_{r=1}^N \left(\hat{p}_r^2 + m^2 \omega^2 \hat{q}_r^2 + 2\tilde{K} (\hat{q}_{r+1} - \hat{q}_r)^2 \right) \end{aligned} \quad (1)$$

where, in getting the second line, we have chosen a scaling $c_0 = 2m$ and also defined the new constant $\tilde{K} = mK$. Periodic boundary conditions are assumed. The operators \hat{p}_i and \hat{q}_i are the usual canonical coordinates with commutation $[\hat{p}_i, \hat{q}_j] = i\hbar$. In our present considerations we focus on the critical (massless) Hamiltonian \hat{H}_0 defined as

$$\hat{H}_0 = \sum_{r=1}^N \hat{p}_r^2 + 2\tilde{K} (\hat{q}_{r+1} - \hat{q}_r)^2, \quad (2)$$

though the non-zero mass case will later be reintroduced. As a free particle system, harmonic lattices are diagonal in the fourier basis. The fourier coordinates, denoted by ‘check’ notation, are defined

$$\begin{aligned} \check{p}_\kappa &= \frac{1}{\sqrt{N}} \sum_{r=1}^N \hat{p}_r e^{-2\pi i r \kappa / N} \\ \check{q}_\kappa &= \frac{1}{\sqrt{N}} \sum_{r=1}^N \hat{q}_r e^{-2\pi i r \kappa / N}. \end{aligned} \quad (3)$$

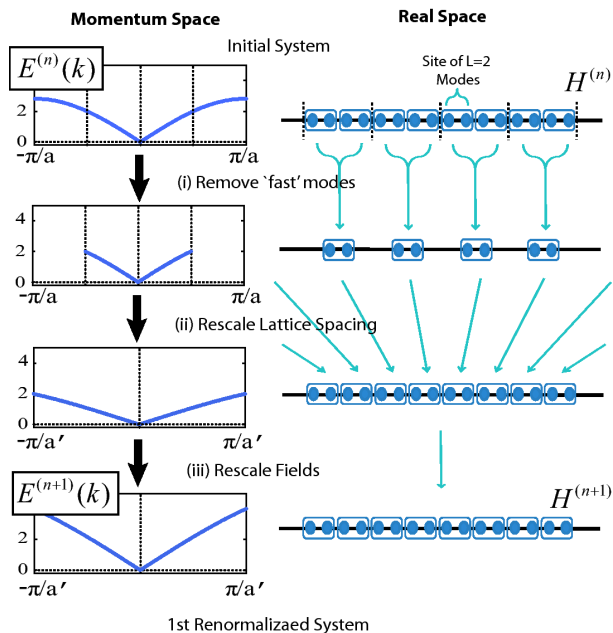


FIG. 2: A comparison of an RG iteration for a $D = 1$ dimensional system (left) in terms of a dispersion relation, $E(k)$, in momentum-space and (right) in terms of a lattice in real-space. It is required, in order to define a proper RG flow in real-space, that the number of modes L in each site remains fixed, i.e. one iteration takes every two sites (4 sites in $D = 2$ spatial dimensions) of L modes into a single site of L modes. Note that the form of the real-space coarse-graining for (i) has been left ambiguous; Fig. (3) describes two non-equivalent ways this step can be realized.

Applying the change of variables brings the original Hamiltonian (2) into diagonal form, here a set of N uncoupled oscillators

$$\hat{H}_0 = \sum_{\kappa=-(N-1)/2}^{(N-1)/2} \tilde{p}_\kappa^2 + 8\tilde{K} \sin^2\left(\frac{\pi\kappa}{N}\right) \tilde{q}_\kappa^2. \quad (4)$$

Defining $k = 2\pi\kappa/(aN)$, with a as the lattice spacing, the thermodynamic limit ($N \rightarrow \infty$) is taken to give

$$\hat{H}_0 = \int_{k=-\pi/a}^{\pi/a} \tilde{p}(k)^2 + 8\tilde{K} \sin^2\left(\frac{ka}{2}\right) \tilde{q}(k)^2 dk. \quad (5)$$

Note that we have a natural momentum cut-off $\Lambda = \pm\pi/a$ originating from the finite lattice spacing; taking the spacing a to zero recovers the real (massless) scalar field. Two equivalent representations of the system have been obtained; (2) in terms of spatial modes (attenable to numeric, real-space RG) and (5) in terms of momentum modes (attenable to analytic, momentum-space RG). The *dispersion relation* (the energy of mode k) for (5) is given as

$$E_0(k) = 2\sqrt{2}\tilde{K} |\sin(ka/2)|. \quad (6)$$

We shall compare the renormalized theories, both in the sense of examining how a particular Hamiltonian is changing along the RG flow and also in the sense how well the momentum-space and real-space results agree, by comparing the corresponding dispersion relations.

III. MOMENTUM-SPACE RG

In this section the harmonic system in the fourier basis (5) is renormalized using momentum-space RG. The RG iteration is broken into three steps. (i) Firstly the cut-off is reduced, $\Lambda \mapsto \Lambda' = \Lambda/s$, with modes greater than the cut-off integrated out to obtain a renormalized Hamiltonian, aimed to preserve a good description of the slow mode physics. Since there is no interaction between the (momentum) modes in the system this step is presently very simple; the cut-off is reduced $\Lambda \mapsto \Lambda' = \Lambda/2$ whilst leaving the form of the Hamiltonian for modes with momentum $k < \Lambda'$ unchanged, giving

$$\hat{H}'_0 = \int_{k=-\pi/2a}^{\pi/2a} \tilde{p}(k)^2 + 8\tilde{K} \sin^2\left(\frac{ka}{2}\right) \tilde{q}(k)^2 dk. \quad (7)$$

(ii) Next the length associated to the system is changed; implemented as a scaling of the lattice spacing¹, $a \mapsto a' = 2a$, giving

$$\hat{H}''_0 = \int_{k=-\pi/a'}^{\pi/a'} \tilde{p}(k)^2 + 8\tilde{K} \sin^2\left(\frac{ka'}{4}\right) \tilde{q}(k)^2 dk. \quad (8)$$

Here we have made a change in the observation scale of the system in terms of length, in order to have the notion of invariance a corresponding change in the *energy scale* is made. In the final step (iii) the fields are rescaled

$$\begin{aligned} \tilde{p}(k) &\mapsto \tilde{p}'(k) = \frac{1}{\sqrt{2}}\tilde{p}(k) \\ \tilde{q}(k) &\mapsto \tilde{q}'(k) = \frac{1}{\sqrt{2}}\tilde{q}(k). \end{aligned} \quad (9)$$

The new field operators have a modified commutation relation $[p'(k), q'(k)] = i\hbar/2$, in accordance with the desire for a change of energy scale. In principle the RG iteration is complete, however in this particular case a further transform is required in order to make manifest the invariance of the critical Hamiltonian; new field operators

¹ the approach of rescaling the lattice spacing is common in the context of condensed matter problems; equivalently we could have rescaled the momentum of the theory, $k \mapsto k' = 2k$, as is the approach most often used for the RG in a quantum field theory setting

are defined

$$\begin{aligned}\hat{p}' &\mapsto \hat{p}'' = \sqrt{2}\hat{p}' \\ \hat{q}' &\mapsto \hat{q}'' = \frac{1}{\sqrt{2}}\hat{q}'.\end{aligned}\quad (10)$$

Note that, in contrast to the previous transform (9), this transform is *commutation preserving* hence will not affect the relevant physics of the system; namely the dispersion relation remains unchanged. Implementing the third step (together with the auxiliary transform (10)), the first renormalized Hamiltonian, $\hat{H}_0^{(1)}$, is given

$$\hat{H}_0^{(1)} = \int_{k=-\pi/a'}^{\pi/a'} \hat{p}''(k')^2 + 32\tilde{K} \sin^2\left(\frac{ka'}{4}\right) \hat{q}''(k')^2 dk. \quad (11)$$

The RG iteration is summarized: (i) degrees of freedom not relevant to the low energy physics are removed, followed by a changes in observation scale in terms of (ii) *length* ($a \mapsto a' = 2a$) and (iii) *energy* ($\hbar \mapsto \hbar' = \hbar/2$). Of course the scale factors chosen in (ii) and (iii) may depend on the implementation of the RG as well as the problem to which it is being applied. Iterating the RG transform (dropping the ‘primes’ from notation), the n^{th} renormalized Hamiltonian is given as

$$\begin{aligned}\hat{H}_0^{(n)} &= \int_{k=-\pi/a}^{\pi/a} \hat{p}(k)^2 + 2^{2n+3}\tilde{K} \sin^2\left(\frac{ka}{2^{n+1}}\right) \hat{q}(k)^2 dk \\ &= \int_{k=-\pi/a}^{\pi/a} \hat{p}(k)^2 + \tilde{K}(k^2 a^2 + O(2^{-2n})) \hat{q}(k)^2 dk\end{aligned}\quad (12)$$

which clearly tends to a fixed point of the RG flow (i.e. is convergent in the large n limit). Of course the corresponding dispersion relations also tend to a fixed point

$$\begin{aligned}E_0^{(n)}(k) &= 2^{n+\frac{3}{2}}\sqrt{\tilde{K}}|\sin(ka/2^{n+1})| \\ &= a\sqrt{2\tilde{K}}|k| + O(2^{-2n}).\end{aligned}\quad (13)$$

Here we have an example where the fixed point gives a *linear* dependence of energy on momentum.

Note that a key conceptual point here was that at each iteration we are mapping Hamiltonians, defined in terms of couplings in some parameter space, to new coarse-grained Hamiltonians in *the same* parameter space; in this way the RG flow of Hamiltonians (or couplings) can be described. This is an important point; critical systems, like the massless system considered here, are often seen to be (non-trivial) fixed points of the RG flow and we can classify perturbations to the critical theory as being relevant or irrelevant by whether deviations from fixed point (induced by the perturbations) grow or diminish under the RG flow. Examples of relevant and irrelevant perturbations are given in the following sections.

A. Relevant perturbation

A mass term, H_{Rel} , is reintroduced to the critical system (6) in the context of being a *relevant perturbation*; this is a term that *grows* under RG iteration hence significantly modifies the system asymptotics from the unperturbed system. The mass term is diagonal in both real-space and fourier-space representations

$$\hat{H}_{\text{Rel}}^{(0)} \equiv \sum_r \hat{q}_r^2 = \int_{k=-\pi/a}^{\pi/a} \hat{q}(k)^2 dk. \quad (14)$$

It is seen that the perturbed Hamiltonian, $\hat{H} = \hat{H}_0 + m^2\hat{H}_{\text{Rel}}^{(0)}$, is equal to the original Hamiltonian (1); we are again dealing with coupled oscillators of mass m . Since this perturbation term does not reorder modes ($E(k)$ is still increasing function of $|k|$) we may perform the same RG transformations as on the unperturbed system which gives

$$\hat{H}_{\text{Rel}}^{(n)} = 2^{2n}\hat{H}_{\text{Rel}}^{(0)}. \quad (15)$$

The mass term is seen to term grow exponentially under RG iteration; as such, choosing even a small m will lead to markedly different behavior in the appropriate low-energy regime. This is evidenced by the dispersion relation, $E_R^{(n)}$, of the perturbed system

$$\begin{aligned}E_R^{(n)}(k) &= 2^n \sqrt{m^2 + 8\tilde{K} \sin^2(ka/2^{n+1})} \\ &= 2^n m + \frac{a^2\tilde{K}}{2^n m} k^2 + O\left(\frac{a^2\tilde{K}}{m^3 2^{3n-3}}\right).\end{aligned}\quad (16)$$

Comparing with (13), which tended to a linear dispersion, we now see a quadratic dependence of energy on momentum k together with an energy-gap that grows *exponentially* with RG iteration.

B. Irrelevant perturbation

Perturbations to the system that get smaller under RG flow are deemed *irrelevant perturbations* as these to not affect the asymptotic, low-energy behavior of the system. An example of such a perturbation can be constructed in real-space from local quadratic couplings, hence is again diagonal in fourier-space representation

$$\begin{aligned}\hat{H}_{\text{Irrel}}^{(0)} &\equiv \sum_{r=1}^N -\hat{q}_r^2 + (\hat{q}_{r+1} - \hat{q}_r)^2 + \frac{1}{4}(\hat{q}_{r+2} + \hat{q}_r)^2 \\ &= 4 \int_{k=-\pi/a}^{\pi/a} \sin^4\left(\frac{ka}{2}\right) \hat{q}(k)^2 dk.\end{aligned}\quad (17)$$

In considering the perturbed system $\hat{H} = \hat{H}_0 + \alpha\hat{H}_{\text{Irrel}}$, if we choose $\alpha > -1$ then the mode energy remains an

increasing function of momentum $|k|$; this allows the use of the same RG transforms as the unperturbed case to get

$$\begin{aligned}
 H_{\text{Irrel}}^{(n)} &= \int_{k=-\pi/a}^{\pi/a} 2^{2n+2} \sin^4\left(\frac{ka}{2^{n+1}}\right) \hat{q}(k)^2 dk \\
 &\approx 2^{-2n-2} a^4 \int_{k=-\pi/a}^{\pi/a} k^4 \hat{q}(k)^2 dk.
 \end{aligned} \tag{18}$$

It is seen that the addition of the perturbation H_{Irrel} to the critical Hamiltonian has diminishingly small effect on the low-energy behavior, reinforced by the dispersion $E_{\text{IR}}^{(n)}$ of the perturbed system

$$\begin{aligned}
 E_{\text{IR}}^{(n)}(k) &= 2^{n+1} \left| \sin\left(\frac{ka}{2^{n+1}}\right) \right| \sqrt{2\tilde{K} + \alpha \sin^2\left(\frac{ka}{2^{n+1}}\right)} \\
 &= a\sqrt{2\tilde{K}} |k| + O(2^{-2n})
 \end{aligned} \tag{19}$$

which possess the same large- n behavior of the unperturbed system (13).

IV. REAL-SPACE RG

In this section method for applying the numeric, real-space RG is described. Before performing the RG, the lattice is partitioned local groups of L modes henceforth referred to as *sites*. Each RG iteration is to map a block, composed of 2 sites (or 2^D sites in D -dimensions), into a single effective site in the coarse-grained lattice. A desired property of the transform is that the effective sites in the coarse-grained lattices are also composed of L bosonic modes. This is necessary in order to retain the notion of a *proper* RG flow; with this condition fulfilled the RG transform is a mapping from Hamiltonians defined on an initial lattice to a coarse-grained Hamiltonian defined on an identical lattice, allowing for meaningful comparison of the theories. Keeping a constant L also results in a *sustainable* RG transform that can, in principle, be iterated an arbitrary number of times. Allowing for growth in L between RG iterations results in growth of computational expense in performing the transform, limiting the times the RG may be iterated. In the present setting the value L is seen to be an (adjustable) accuracy parameter. Choosing L larger allows for a more accurate results but is more computationally expensive; indeed in a general application of a real-space blocking method the computational expense grows exponentially with the modes per site L .

The coarse-graining step, in which a block of two sites is mapped into the single effective site, may be accomplished in different ways. Considered here are a local projection (LP) method and entanglement renormalization (ER); these are detailed Fig. (3). The LP may be seen as

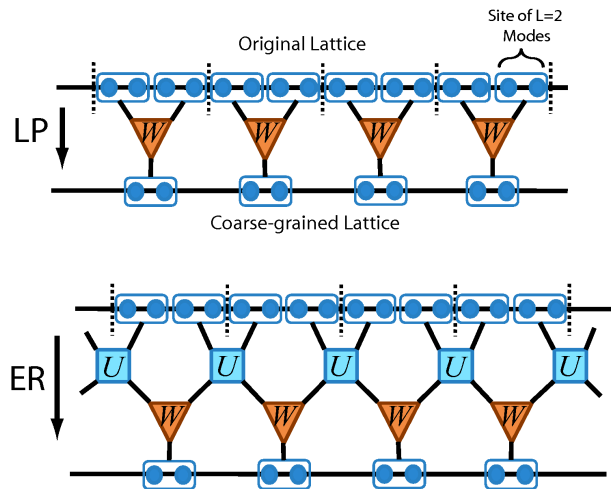


FIG. 3: The first step of the real-space RG, in which 2^D sites (each composed of L modes) of the original D -dimensional cubic lattice is mapped to a single site of the coarse-grained lattice, can be accomplished in different ways. (Top) The simplest method involves a series of local projections, realized by isometric tensors W , to implement the coarse-graining, as depicted for the 1D lattice. This shall subsequently be referred to as the local projection (LP) method. (Bottom) The inclusion disentangler tensors U in the coarse-graining gives the method of entanglement renormalization (ER).

a simplification of ER in which we restrict the disentangler transformations U to being identity transformations; hence only the latter (more complicated) method shall be described explicitly. For clarity we discuss the implementation of the RG in terms of a 1D chain of N modes with periodic boundary conditions, though in practice we take the system size to be infinite and have also analyzed 2D lattices with a similar method.

A. Hamiltonian RG

1. Operator Algebra

Defining a quadrature vector $\vec{R} \equiv (\vec{p}, \vec{q})$ with

$$\vec{p} \equiv \begin{pmatrix} \hat{p}_1 \\ \hat{p}_2 \\ \vdots \\ \hat{p}_N \end{pmatrix}, \vec{q} \equiv \begin{pmatrix} \hat{q}_1 \\ \hat{q}_2 \\ \vdots \\ \hat{q}_N \end{pmatrix} \tag{20}$$

it is seen that the Hamiltonians (1) under consideration may be written in *quadratic form*

$$\hat{H} = \sum_{i,j=1}^{2N} R_i^T \mathcal{H}_{ij} R_j \tag{21}$$

where \mathcal{H} , henceforth referred to as the Hamiltonian matrix, is a $2N \times 2N$ hermitian matrix. That the systems

under consideration only contain quadratic couplings can be exploited to allow a more efficient realization of ER; one in which the RG is carried in the space of \mathcal{H} . This entails limiting to transformations (i.e. the disentanglers and isometries which comprise ER) to those which map the system of bosonic modes to another system of bosonic modes; in other words *commutation preserving* transformations. The reader is reminded that although the procedure described here will not be applicable outside of the quadratic setting, the more general approach to ER in terms of the full Hamiltonian \hat{H} could still be efficiently implemented. If the Hamiltonian matrix is transformed $\mathcal{H} \mapsto \mathcal{H}' = S^T \mathcal{H} S$ we require S to be a symplectic transform, $S \in \text{Sp}(2N, \mathbb{R})$. Symplectic transforms can be characterized as those which leave the symplectic matrix Σ invariant under conjugation, $S^T \Sigma S = \Sigma$. Under our grouping of the quadrature vectors (20) the symplectic matrix takes the form

$$\Sigma \equiv \begin{pmatrix} 0 & \mathbb{I}_N \\ -\mathbb{I}_N & 0 \end{pmatrix} \quad (22)$$

with \mathbb{I}_N as the $N \times N$ identity. Additionally, the systems under consideration take even simpler form than (21); we may write the relevant Hamiltonians as $\hat{H} = \vec{p}^T \mathcal{H}_p \vec{p} + \vec{q}^T \mathcal{H}_q \vec{q}$ with the kinetic part of the Hamiltonian as the identity, $\mathcal{H}_p = \mathbb{I}_N$. This implies that only symplectic transforms S which are of the form $S = V \oplus V$, with V a *special orthogonal* transformation, $V \in \text{SO}(2N)$, need be considered. It is easily checked that $V \oplus V$ is a symplectic transform, in fact this is an element of the maximal compact subgroup of $\text{Sp}(2N, \mathbb{R})$.

2. Transforming the Hamiltonian

The real-space RG transform, as generated by ER, is realized by a series of local symplectic transforms, the disentanglers and isometries, on the Hamiltonian matrix. Each RG transform is to map a block, composed of 2 sites, from the original lattice to single site in coarse-grained lattice. To this end the disentanglers U are realized as special orthogonal transforms, $U \in \text{SO}(2L)$, which act across the boundaries of neighboring blocks. Isometries, W , are realized as a composition of a special orthogonal transform followed by a projection which act within a block. That is $W = RY$ with $R \in \text{SO}(2L)$ and the projection $Y = (0_L \oplus \mathbb{I}_L)$. It is desired that the disentanglers and isometries be optimized to project onto the *minimum* energy subspace of the original Hamiltonian; a variational method to find good disentanglers and isometries for achieving this goal is described in appendix A.

Assuming the disentanglers U and isometries W have been obtained, the procedure for an iteration of real-space RG is broken into 3 steps, as depicted Fig. (4), analogous to the momentum-space procedure. (i) Firstly the Hamiltonian matrix is transformed with the disentanglers and isometries. The kinetic part of the Hamiltonian matrix is trivial, $\mathcal{H}_p = \mathbb{I}_N$, and remains so under

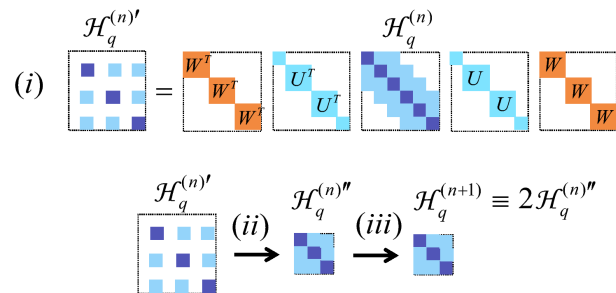


FIG. 4: An iteration of entanglement renormalization, broken into three steps, is depicted in terms of the direct sum structure of the Hamiltonian matrix \mathcal{H}_q . Dark shaded squares in \mathcal{H}_q represent couplings within the site of L modes, light shaded squares are the couplings between sites (at most next-to-nearest neighbour). Step(i), removing ‘fast’ modes is realized by transforming \mathcal{H}_q by conjugation with the disentanglers U and isometries W . Step(ii), rescaling the momentum, is achieved by removing the zero rows/columns from \mathcal{H}_q' . Step(iii) is rescaling the fields, and here amounts to scaling \mathcal{H}_q'' by a factor of 2. These three steps combined take the n^{th} renormalized Hamiltonian matrix $\mathcal{H}_q^{(n)}$ to the $(n+1)^{\text{th}}$ renormalized Hamiltonian matrix $\mathcal{H}_q^{(n+1)}$.

the transformations considered, hence may be neglected. The relevant (q -quadrature) part of the initial Hamiltonian $\mathcal{H}_q^{(0)}$ transforms as

$$\mathcal{H}_q^{(0)'} = (\oplus W_1^T)(\oplus U_1^T)\mathcal{H}_q^{(0)}(\oplus U_1)(\oplus W_1) \quad (23)$$

where it is again understood that disentanglers act *between* blocks whilst isometries act *within* blocks, depicted Fig. (4). (ii) Next zero rows/columns are removed from Hamiltonian matrix to form a the new matrix $\mathcal{H}_q^{(0)''}$. (iii) The final step, rescaling fields, is realized by scaling the Hamiltonian matrix. Here the same rescaling as Eqns. (9) and (10) is realized as $\mathcal{H}_q^{(1)} \equiv 2\mathcal{H}_q^{(0)''}$, with $\mathcal{H}_q^{(1)}$ as the first renormalized Hamiltonian. Iterating this procedure n times obtains the n^{th} renormalized Hamiltonian $\mathcal{H}_q^{(n)}$. Note that, as a direct consequence of the bounded causal structure of the ER transform [9], if the original Hamiltonian $\mathcal{H}^{(0)}$ translationally invariant in sites, containing local interactions (at most between neighbouring and next-to-neighbouring sites), then the coarse-grained Hamiltonians $\mathcal{H}^{(n)}$ will also be translationally invariant in sites with at most next-to-neighbouring interactions.

B. Ground-State RG

Up until this section only RG transforms of Hamiltonians have been considered; also possible is real-space transforms of *states* on the lattice. Having described the methods of Hamiltonian RG in momentum-space and in real-space, we could proceed straight to comparison of results; however it will be instructive to beforehand con-

sider ground-state RG as the results from this section will later complement the Hamiltonian RG results. The notion of coarse-graining ground states is also a very relevant part of efficient simulation algorithms with ER [13]. Ground-state RG proceeds similar to that of the Hamiltonian RG, by iteratively removing short-range degrees of freedom one can investigate the long-range behavior of the state. It should be noted that, in contrast to the Hamiltonian RG which loses information about the high-energy spectrum at each iteration, we do not necessarily lose any information about the ground-state with the RG. This is taken in the sense that, from a coarse-grained state together with knowledge of the RG transforms it was produced from, we can regain the original state up to some finite accuracy. In this way the network of disentanglers and isometries that result from the transforms specify an efficient representation of a class of states; this is known as the multi-scale entanglement renormalization ansatz (MERA). Here, as our system is solvable, we start from exact ground-state and build the MERA approximation to the ground-state through iterative RG transforms; one advantage of this approach is it allows one to keep track of errors introduced at each step. In a more general, non-solvable model one could start by assuming the ground-state may be approximated as a MERA and then use a variational method to optimize the approximation.

The ground-state RG is started from an exact representation of the ground-state in terms of a covariance matrix, $\gamma = \gamma_p \oplus \gamma_q$, defined as

$$\begin{aligned} (\gamma_p)_{ij} &\equiv 2 \langle \psi_{\text{GS}} | \hat{p}_i \hat{p}_j | \psi_{\text{GS}} \rangle \\ (\gamma_q)_{ij} &\equiv 2 \langle \psi_{\text{GS}} | \hat{q}_i \hat{q}_j | \psi_{\text{GS}} \rangle. \end{aligned} \quad (24)$$

The derivation and analytic expressions for γ_p , γ_q are described in appendix B. Similar to the approach taken in the Hamiltonian RG, the ER transformation of the ground-state shall be realized by symplectic transforms acting the space of the covariance matrix, $\gamma \mapsto \gamma' = S^T \gamma S$. Here, since both γ_p and γ_q are non-trivial, a larger subgroup of $\text{Sp}(2N, \mathbb{R})$ is required than used for the Hamiltonian RG. The relevant symplectic transforms S are of the form $S = A \oplus (A^{-1})^T$ with A any $N \times N$ invertible matrix. The covariance matrices transform by conjugation

$$\begin{aligned} \gamma_p &\mapsto \gamma'_p = A^T \gamma_p A \\ \gamma_q &\mapsto \gamma'_q = A^{-1} \gamma_q (A^{-1})^T \end{aligned} \quad (25)$$

In this way disentanglers, \tilde{U} , are realized as invertible $2L \times 2L$ matrices which transform the ground-state in the same way as matrix A above. Isometries \tilde{W} are realized as $\tilde{W} = \tilde{R}Y$, with \tilde{R} an invertible $2L \times 2L$ matrix and the projection Y , as previously defined $Y = (0_L \oplus \mathbb{I}_L)$.

For the RG transform of the ground-state we wish to identify and remove short-range degrees of freedom, equivalently these may be characterized as modes within a block that are *unentangled* with the rest of the system outside of the block. The relation between removing

modes from the description of the system as a means of truncating the Hilbert space is explored, in terms of fermionic modes, in the appendix of [10]. For a block of $2L$ modes from the covariance matrix, we may associate $2L$ symplectic eigenvalues, λ_i with $i = 1 \cdots 2L$, defined as

$$\lambda_i = \text{Spect} \{ (\gamma_p)|_{2L} (\gamma_q)|_{2L} \}. \quad (26)$$

Note that the uncertainty relation, which may be simplified here as $\langle \hat{p}^2 \rangle \langle \hat{q}^2 \rangle \geq 1/4$, enforces that $\lambda_i \geq 1$ for all i , with equality holding only when the corresponding mode has minimum uncertainty. The only minimum uncertainty Gaussian state that a mode can be in is a single-particle the ground-state; equivalently identifying a mode i that has $\lambda_i = 1$ ensures that the mode is uncorrelated with other modes in the system. Such modes, which form a product state with the rest of the system, may be projected out via the RG transform without introducing error.

The disentanglers and isometries which comprise the RG are optimized with this idea in mind; we wish to minimize the eigenvalue λ_i of the modes to be projected out. A matrix equation for this minimization can be written

$$\min_{\tilde{R}, \tilde{U}} \text{tr} \{ \gamma'_p \gamma'_q (\mathbb{I}_{2L} - Y) \} \quad (27)$$

with γ'_p and γ'_q as the coarse-grained covariance matrices as transformed by applying the ER

$$\begin{aligned} \gamma'_p &= \tilde{R}^T (\tilde{U}^T \oplus \tilde{U}^T) (\gamma_p)_{6L} (\tilde{U} \oplus \tilde{U}) \tilde{R} \\ \gamma'_q &= \tilde{R}^{IT} (\tilde{U}^{IT} \oplus \tilde{U}^{IT}) (\gamma_q)_{6L} (\tilde{U}^{-1} \oplus \tilde{U}^{-1}) \tilde{R}^{-1}. \end{aligned} \quad (28)$$

and R^{IT} as shorthand for $(R^{-1})^T$. Note that if Y projects on the subspace to be kept, then $(\mathbb{I}_{2L} - Y)$ projects onto the subspace to be removed. Eqn. (27) can again be optimized to find good disentanglers and isometries, with alternating improvements for \tilde{U} and \tilde{W} , similar to that described in the appendix A for the Hamiltonian RG.

As stated earlier, the sequence of disentanglers $\{\tilde{U}^{(1)}, \tilde{U}^{(2)} \dots\}$ and isometries $\{\tilde{W}^{(1)}, \tilde{W}^{(2)} \dots\}$ obtained through successive RG transforms comprise the MERA for the ground-state, through which expectation values for the ground-state may be computed. In practice the modes removed will not be entirely decoupled from the system, $\lambda_i = 1 + \epsilon_i$, which will introduce some errors into the MERA representation. An upper bound for the error on any two-point correlation is given as $\max(\sqrt{\epsilon_i})$, though individual errors in correlations are usually significantly smaller.

The entropy of entanglement shall be used as a measure to compare how ground-states are changing along the RG flow. The entropy for the block of $2L$ modes within the lattice [15] is precisely the sum of the entropy

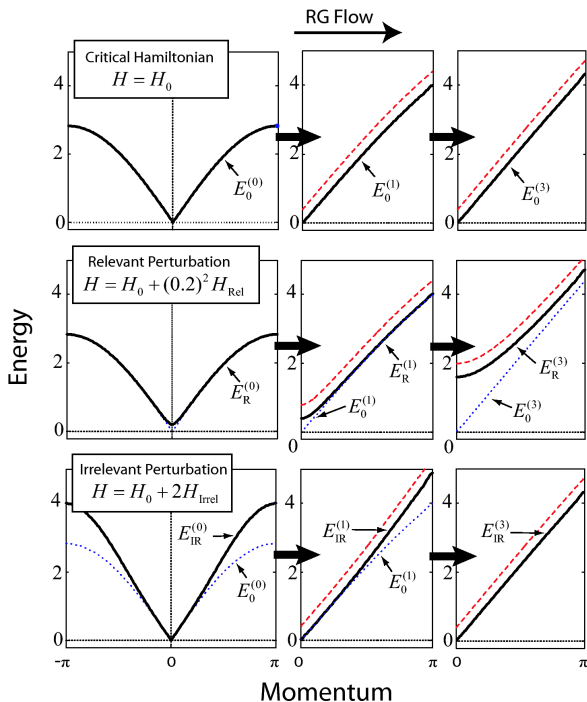


FIG. 5: Sequences of dispersion relations of Hamiltonians and after $n = 0, 1, 3$ RG transforms, comparing the real-space ER results (bold) with the exact momentum-space results (dashed, offset by 0.2). (Top Series) The critical Hamiltonian renormalized with ER tends to a fixed point of the RG flow, in good agreement with momentum-space results. (Middle Series) Adding a small mass, $m = 0.2$, to the critical system gives a marked difference in the dispersion relation after $n = 3$ RG transforms. (Bottom Series) The effect of an irrelevant perturbation quickly diminishes under RG flow; by $n = 3$ iterations the original and the perturbed dispersions are visually identical, $E_{\text{IR}}^{(3)} \approx E_0^{(3)}$.

of the uncorrelated modes within the block, here specified in terms of the symplectic eigenvalues λ_i

$$S_{2L} = \sum_{i=1}^{2L} \left[f\left(\frac{\sqrt{\lambda_i} - 1}{2}\right) - f\left(\frac{\sqrt{\lambda_i} + 1}{2}\right) \right] \quad (29)$$

with $f(x) = -x \log x$.

V. RESULTS AND DISCUSSION

Figs. (5) shows a comparison of analytic and numeric dispersion relations for the critical 1D lattice and perturbations thereof. Analytic results were obtained from momentum-space RG, Eqns. (13), (16) and (19), without any approximation, whilst numeric results are from real-space RG performed with entanglement renormalization. The results from the ER method approximate exact results with accuracy as to be visually indistinguishable for the sequence of three RG transforms performed. Im-

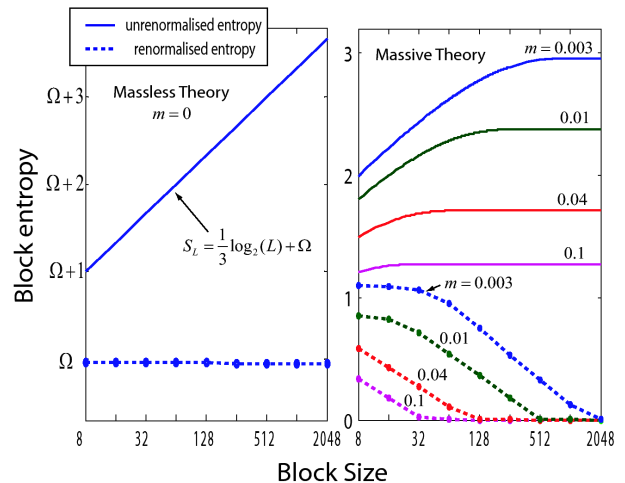


FIG. 6: Block entropy along RG flow of the ground-state in 1D. (Left) In the critical (massless) regime the entropy of a block of finite length becomes infinite, as realized by the infinite constant Ω ; however we can still make sense of *changes in entropy* via a limiting process (see appendix B). The unrenormalized entropy scales logarithmically, in agreement with results from conformal field theory, whilst entropy of the system renormalized with entanglement renormalization remains constant along the RG flow. In fact, the critical ground-state is a fixed point of RG flow induced by ER; the sequence of renormalized ground-states $\{\gamma^{(1)}, \gamma^{(2)}, \dots\}$ rapidly converge to a fixed γ^* . (Right) For several values of finite mass, the unrenormalized entropy saturates at a length scale governed by correlation length, whilst the theories renormalized with ER factorize into a product state at the approximately same length.

portant is that the real-space method with ER is able to reproduce expected behavior from RG in terms of critical fixed points, relevant and irrelevant perturbations. The numeric results were produced taking $L = 6$ modes per site.

The entropy plots from the ground-state renormalization Fig. (6) are seen to complement the Hamiltonian RG results Fig. (5) with a new perspective. As the critical Hamiltonian rapidly converged to a fixed point of the RG flow; so does the corresponding ground-state. The sequence of successively coarse grained ground-states, represented as covariances matrices, $\{\gamma^{(1)}, \gamma^{(2)}, \dots\}$ converged to the fixed point $\gamma^{(n)} = \gamma^*$ for $n \geq 3$. Aside from being conceptually satisfying, capturing the scale invariance of the system leads to numerical gains. The MERA approximation to the ground-state is formed of the sequence of disentangles $\{U_1, U_2, U_3, \dots\}$ and isometries $\{W_1, W_2, W_3, \dots\}$ from the RG; the scale invariance gives $U^{(n)} = U^{(3)}$ for $n > 3$ and likewise for isometries. Combined with translational invariance, this leads to an extremely compact description of the ground-state, through which expectation values may be calculated, in terms of only 3 unitary and 3 isometric matrices. In the non-zero mass cases the ground-state flows to a trivial point of the

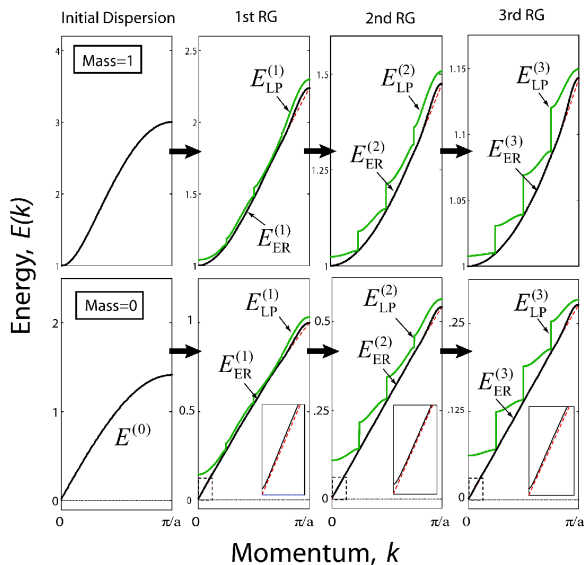


FIG. 7: (Left) Sequences of dispersion relations (in non-rescaled energy units) for the gapped (top) and critical (bottom) 1D systems after $n = 0, 1, 2, 3$ real-space RG transforms, comparing the results from the local projection method, $E_{LP}^{(n)}$, to those from coarse-graining with entanglement renormalization, $E_{ER}^{(n)}$. The coarse-graining performed with entanglement renormalization captures the low-energy subspace of the theory to good approximation; the numeric data agrees with the exact low-energy subspace obtained from momentum-space RG (dashed) as to be almost visually indistinguishable. Though the spectrum obtained from ER does have small errors, as can be seen in the insets and also noticeable near the momentum cut-off, $k = \pi/a$. An equivalent optimization performed without disentanglers, the local projection (LP) method, is seen to be a poor approximation to the low-energy theory after a few RG transforms. Note that the numeric RG was performed keeping $L = 4$ modes per site at each iteration.

RG, a product state, at a length scale close to the correlation length of the system. That is, say for instance in the $m = 0.1$ case, we have sequence of coarse-grained ground states $\{\gamma^{(1)}, \gamma^{(2)}, \gamma^{(3)}, \dots\}$, where state $\gamma^{(3)}$ (and successive coarse-grained ground-states) are product states, as indicated by the system having zero block-entropy. This is consistent with the growth of the mass-gap observed in the finite-mass case of the Hamiltonian RG; a system with a large mass gap would be expected to have a ground-state that is indeed a product state. This feature of gapped systems under transforms with ER leads to improved numerical efficiency; the MERA representation of the infinite ground-state may be completely specified by the disentanglers and isometries from the first few RG transforms until the product state is reached. The ground-state coarse-graining was performed with $L = 4$ modes per site. The critical system was the most computationally demanding, having maximum truncation error $\epsilon_r = 1 \times 10^{-4}$ and an energy error of 0.0034 after 9 RG iterations.

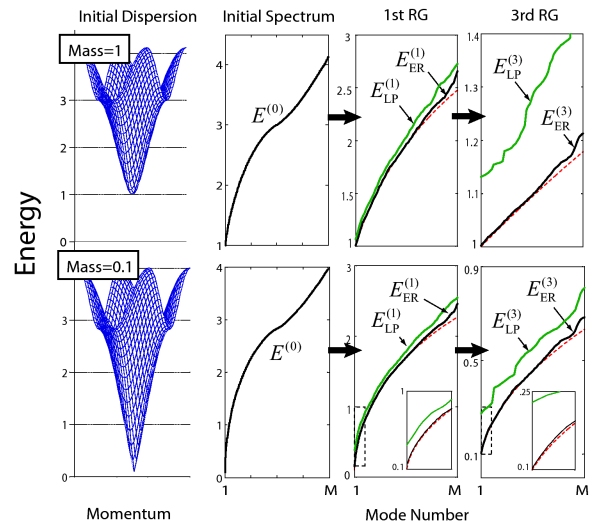


FIG. 8: Sequences of energy spectra (in non-rescaled energy units) for gapped (top) and near-critical (bottom) 2D infinite lattice systems after $n = 0, 1, 3$ real-space RG transforms. Again the performance of the numeric real-space methods, local projection (LP) and entanglement renormalization (ER), are benchmarked against the exact solutions from momentum-space RG (dashed). The energy spectra are obtained by sampling the dispersion relation $E(k_1, k_2)$ on a finite grid of M points for then ordering the values, $\{E_1 \leq E_2 \leq \dots \leq E_M\}$. The spectra of the systems renormalized with entanglement renormalization, $E_{ER}^{(n)}$, again prove a significantly more accurate approximation to the low-energy theory than that of the method without disentanglers, $E_{LP}^{(n)}$. The divergences of the ER spectra from the exact results are most significant in the (unimportant) high-energy part of the spectra; the desired low-energy spectra remains in good approximation throughout the RG iterations considered. The numeric RG was performed keeping $L = 9$ modes per site.

In Figs. (7), (8) we see a visual comparison of numeric results, in terms of dispersion relations and energy spectra, of the real-space RG, from both the local projection (LP) method and from ER, against exact momentum space results. Even for a small number of RG iterations the spectra from the LP method diverge significantly from the exact spectra; furthermore these errors are seen to grow quickly with increasing RG iterations. Coarse-graining with ER is seen to keep significantly better support of the low energy subspace of the original Hamiltonian; both in terms of the shape of the spectra and the magnitude of the energy values. However, a common feature seen in the numeric spectra obtained with ER is a loss of accuracy towards the high-energy cut-off, Λ . Whilst this may result from difficulty of enforcing a sharp cut-off numerically, this is of little concern as the primary interest lies in the physics near the ground-state not the high-energy cut-off of the effective theory. Fig. (9) presents a comparison of the accuracy of the numeric methods in a more quantitative fashion. In keeping

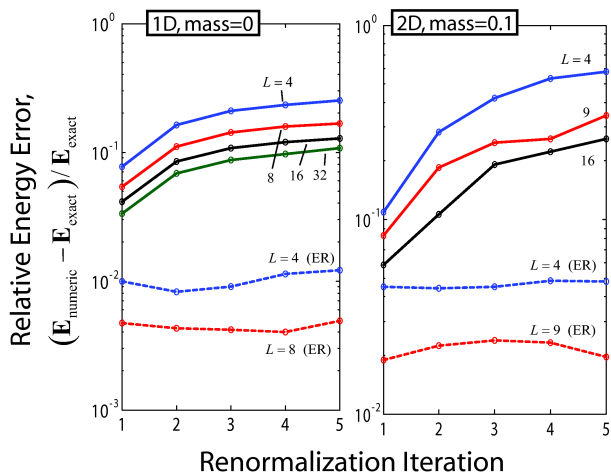


FIG. 9: The numeric RG algorithms are optimized such that the mean energy, defined $\mathbf{E} \equiv \frac{1}{2\Lambda} \int_{-\Lambda}^{\Lambda} E(k) dk$ in 1D and similar for 2D, of the renormalized Hamiltonians is minimized; the goal being to retain the low-energy subspace of the original theory. The difference between the mean energies from the numeric and exact RG is used to quantify the performance of the numeric algorithms; results from LP method are plotted as *solid* lines whilst those from ER are *dashed* lines. (left) For the 1D critical system, the mean of the spectrum obtained from renormalizing with ER, keeping $L = 4$ modes per site, remains approximately 1% greater than the mean energy of the exact low energy subspace throughout the RG iterations. The spectra from the LP method, even when using significantly L , only gives at best 10% accuracy after the same number of RG iterations. (right) For the 2D near critical system, ER gives accuracies no less than 4% and 2% for $L = 4$ and $L = 9$ respectively; this is in contrast to the method without disentanglers which is only accurate to within 60% for $L = 4$ and 30% for $L = 9$. Note an important feature is that, barring small fluctuations, the accuracy of the coarse-graining with ER remains relatively stable with RG iteration.

with the goal of investigating low energy part of original Hamiltonian, the numeric real-space RG algorithms are optimized such as to project onto subspace of Hamiltonian with minimum average energy. One can assess how well the numeric methods are working by comparing this average energy with the exact value from momentum-space results; this comparison between the LP and ER methods is plotted for several values of the accuracy parameter L . Important is that entanglement renormalization is able to induce an RG flow that retains approximately constant accuracy over repeated RG iterations in both the 1D and 2D systems investigated, in principle this allows for exploration of arbitrarily small length scales (or arbitrarily large distances). The local projection method gives less accurate spectra after the first RG iteration and shows increase in error with RG iteration; indeed almost an exponential growth of errors is seen. In the 2D case with $L = 4$ modes per site, the effective

theory obtained with ER has 4% greater energy than the exact minimal energy subspace after 5 RG iterations, the equivalent result from LP has 60% greater energy. Also of note is the relatively poor scaling of the accuracy of these results with the parameter L , even the $L = 16$ results from LP method are significantly less accurate than the $L = 4$ with ER. In coarse-graining a more general system than the harmonic lattices considered, a system in which the diagonalization cannot be performed in terms of the $2L \times 2L$ coefficient matrix, the computational cost of either numeric method will scale exponentially with L , rendering large L simulations computationally unaffordable. We believe that the impressive numerical gains achieved with the use of disentanglers (as with entanglement renormalization) justifies the extra complexity that is imparted to the RG procedure.

It is noted that, for the numeric results, in finding the n^{th} renormalized spectrum the variational method used reoptimized over all previous n RG transforms. For instance, in performing the second RG transform, one would optimize over disentanglers $\{U^{(1)}, U^{(2)}\}$ and isometries $\{W^{(1)}, W^{(2)}\}$ as opposed to only optimizing over $\{U^{(2)}\}$ and $\{W^{(2)}\}$, keeping the disentangler and isometry from the first iteration fixed. This reoptimization over all layers is essential to prevent an exponential growth of errors. For example, say the first numeric RG transform gave errors order ϵ in the theory, even if no further errors were made in the subsequent n RG iterations (without reoptimization of the first RG transform) one would still find errors order $2^n \epsilon$ in the n^{th} renormalized theory due to the *rescaling of the energy* at each RG iteration. Equivalently, as smaller and smaller energy scales are investigated any errors present become more and more significant. It was with this reoptimization that results from ER did not lose accuracy over RG iterations (and in some instances was even more accurate for later RG transforms), though it is noted that even using this method, results from LP still showed large increase in error. The reoptimization comes with the drawback that the variational methods used to find the RG transforms take more iterations to converge for each successive RG transform as a direct result of having to optimize over more parameters.

VI. CONCLUSIONS

In the context of $D = 1, 2$ dimensional harmonic lattices, it has been shown that entanglement renormalization is able to induce a real-space RG transformation that is able to reproduce results from momentum-space RG to a high degree of accuracy over many RG iterations with the degrees of freedom per effective site, L , held a constant. Having a constant L allowed for the definition of fixed points, relevant and irrelevant perturbations in the real-space setting; an important conceptual feature usually only realized in momentum-space RG. A constant L also allowed for a RG transformation that may be sus-

tained over repeated iterations without growth in computational cost. The possibility is opened for using real-space RG, implemented with ER, as a means of investigating the low-energy properties of strongly-correlated systems where perturbative approaches are not valid.

VII. ACKNOWLEDGMENTS

Financial support of the Australian Research Council (APA and FF0668731) is acknowledged.

Appendix. A:- Here a variational method for finding the disentanglers, U , and isometries, W , required for RG with entanglement renormalization, in the situation of Harmonic lattices, is described. Though the details here are specific to the case of Harmonic systems, the variational method is in essence the same as the algorithm for the general case [13]. Alternative variational methods [11] could also be used. Initially every L modes of the lattice is joined into a site, where L for present purposes may be thought of as an adjustable accuracy parameter. An RG iteration is to map a block of two sites to a single effective site in the coarse-grained lattice. In the setting of harmonic lattices, the RG transformation can be performed in the space of the Hamiltonian (coefficient) matrix, \mathcal{H} . Disentanglers U are realized as special orthogonal transforms, $U \in \text{SO}(2L)$, which act across the boundaries of neighboring blocks. Isometries, W , are realized as a composition of a special orthogonal transform followed by a projection which act within a block. That is $W = RY$ with $R \in \text{SO}(2L)$ and the projection $Y = (0_L \oplus \mathbb{I}_L)$. It is desired that the RG transform projects onto the *minimum* energy subspace of the original Hamiltonian, in the present formalism this is given as minimizing the trace of the renormalized Hamiltonian matrix \mathcal{H}' . As a consequence of the translational invariance, it is seen that the trace of the Hamiltonian is the sum of the traces of each of the sites in the Hamiltonian, hence minimizing the trace of a single site in the renormalized theory is equivalent to a minimization carried over the entire Hamiltonian. With $(\mathcal{H}_q)_{4L}$ as a submatrix \mathcal{H}_q for four contiguous sites (a block which is to be disentangled with neighbouring half-blocks), the optimisation may be written as a matrix equation

$$\min_{R,U} \text{tr} \left\{ R^T P_{(4,2)}^T (U^T \oplus U^T) (\mathcal{H}_q)_{4L} (U \oplus U) P_{(4,2)} RY \right\} \quad (30)$$

with $P_{(4,2)}$ as a $4L \times 2L$ projector from the space of four sites to the space of (the middle) two sites. It is not in general possible to solve Eqn. (30) simultaneously for optimal U and R , instead one may use an iterative method based on keeping some terms fixed whilst optimising over others.

To optimize for disentanglers, even whilst holding R constant in (30), the resulting expression contains both terms U , U^T and can not be exactly optimised for U . We proceed by approximating U and U^T as independent

matrices; fixing U^T at some initial value, $U^T = U_i^T$, the optimisation for U may be written

$$\min_{U \in \text{SO}(2L)} \text{tr} \{UB\} \quad (31)$$

where the cyclic property of the trace has been used to bring the U term to the front and B is the product of the remaining terms. The optimization is easier is recast as a maximisation; this is achieved with the inclusion of a minus sign in the argument.

$$\max_{U \in \text{SO}(2L)} \text{tr} \{U(-B + \alpha U_i^T)\} \quad (32)$$

The term αU_i^T , with α an adjustable parameter usually chosen $O(1)$, is added to improve numerical stability; this term enforces that U only undergoes a small change from the initial value U_i with each iteration. Optimizations of the form (32) are solvable; if $(-B + \alpha U_i^T)$ has singular value decomposition $(-B + \alpha U_i^T) = \tilde{U} \tilde{S} \tilde{V}^T$ then optimal choice for disentangler is $U = \tilde{V} \tilde{U}^T$. The optimization for the isometry R in (30) is carried out in the same manner; one alternates the optimizations for disentanglers and isometries until convergence is reach.

It should be noted that, as the optimisation step for disentanglers/ isometries is only approximate, we cannot even be sure that the updated disentangler/ isometry will be better than the previous one. Likewise, there is no guarantee that this optimization will not converge to a local maxima instead of the desired global maxima. Fortunately it is seen that in practice this and similar optimizations work surprisingly well. The variational method required in this work is slightly more complex than the method described here; when computing the n^{th} RG transform we optimize over all n RG transforms, this is the set of disentanglers $\{U^{(1)}, U^{(2)}, \dots, U^{(n)}\}$ and isometries $\{W^{(1)}, W^{(2)}, \dots, W^{(n)}\}$. However each layer may be optimised as shown here, all that changes is the projector Y from (30) is modified to project onto a reduced subspace, and we alternate iterations over the many different layers treating one at a time.

Appendix. B:- Here the ground-state covariance matrices are derived, including the procedure for regularizing the divergent, zero-mass case. The harmonic lattice in the fourier basis (5) consists of N uncoupled oscillators; it follows that the ground-state (in this basis) is a product state of the single oscillator ground-states. The covariance matrix for the state is diagonal with entries corresponding to single oscillator covariances

$$\begin{aligned} \langle \check{p}_{\kappa_1} \check{p}_{\kappa_2} \rangle_{\text{GS}} &= \frac{1}{2} \delta_{\kappa_1, \kappa_2} \sqrt{m^2 \omega^2 + 8 \tilde{K} \sin^2(\pi \kappa_1 / N)} \\ \langle \check{q}_{\kappa_1} \check{q}_{\kappa_2} \rangle_{\text{GS}} &= \frac{1}{2} \delta_{\kappa_1, \kappa_2} \left(1 / \sqrt{m^2 \omega^2 + 8 \tilde{K} \sin^2(\pi \kappa_1 / N)} \right). \end{aligned} \quad (33)$$

The correlators in the original (spatial) basis are derived by substituting in the fourier transform relations (3) giv-

ing

$$\begin{aligned}
(\gamma_p)_{0r} &= \frac{1}{N} \sum_{\kappa=\frac{1-N}{2}}^{\frac{(N-1)}{2}} \cos\left(\frac{2\pi r \kappa}{N}\right) \sqrt{m^2 \omega^2 + 8\tilde{K} \sin^2\left(\frac{\pi \kappa}{N}\right)} \\
(\gamma_q)_{0r} &= \frac{1}{N} \sum_{\kappa=\frac{1-N}{2}}^{\frac{(N-1)}{2}} \frac{\cos\left(\frac{2\pi r \kappa}{N}\right)}{\sqrt{m^2 \omega^2 + 8\tilde{K} \sin^2\left(\frac{\pi \kappa}{N}\right)}}. \quad (34)
\end{aligned}$$

The reader is reminded of the definitions of the covariance matrices used here $(\gamma_p)_{0r} \equiv 2 \langle \hat{p}_0 \hat{p}_r \rangle_{\text{GS}}$ and $(\gamma_q)_{0r} \equiv 2 \langle \hat{q}_0 \hat{q}_r \rangle_{\text{GS}}$. It is possible to take the thermodynamic ($N \rightarrow \infty$) limit, in which the sums will be replaced by an integrals; however, in all but a particular case, to be addressed shortly, the resulting integrals are difficult to evaluate. It is often more convenient, when working on a length scale of at most R modes from the infinite system, to use the finite N equations (34) with $N \gg R$ to in order to approximate the correlators of the infinite system. For the $m = 0$ case it is possible to evaluate the integral equations exactly; taking the thermodynamic limit with $k = \frac{2\pi \kappa}{N}$ gives

$$(\gamma_p)_{0r} = \frac{\sqrt{2\tilde{K}}}{\pi} \int_{k=-\pi}^{\pi} \cos(kr) \left| \sin\left(\frac{k}{2}\right) \right| dk \quad (35)$$

$$(\gamma_q)_{0r} = \frac{1}{4\pi\sqrt{2\tilde{K}}} \int_{k=-\pi}^{\pi} \frac{\cos(kr)}{\left| \sin\left(\frac{k}{2}\right) \right|} dk. \quad (36)$$

It is seen that the integral for the q -quadrature (36) is *divergent*, $(\gamma_q)_{0r} = \infty$ for all r . We proceed by regularizing the integrals with a small momentum cut-off; that is only modes with $|k| > \varepsilon$ are integrated. The limit as $\varepsilon \rightarrow 0$ is then investigated. The p -quadrature integral evaluates as

$$(\gamma_p)_{0r;\varepsilon} = \frac{2\sqrt{2\tilde{K}}}{\pi} \left[\frac{1}{2r+1} - \frac{1}{2r-1} \right] + O(\varepsilon^2 r^2) \quad (37)$$

which is clearly convergent in the $\varepsilon \rightarrow 0$ limit. To evaluate the q -quadrature integral the substitution $x = e^{ik/2}$ is made

$$(\gamma_q)_{0r;\varepsilon} = \frac{1}{\pi\sqrt{2\tilde{K}}} \left[\int_{k=\varepsilon}^{\pi} \frac{x^{2r}}{x^2-1} dx - \int_{k=-\pi}^{-\varepsilon} \frac{x^{2r}}{x^2-1} dx \right]. \quad (38)$$

The integrand is seen to have a finite series expansion

$$\frac{x^{2r}}{x^2-1} = \sum_{s=1}^r x^{2s-2} + \frac{1}{x^2-1}. \quad (39)$$

In this way the q -quadrature divergence manifests in a particularly simple fashion; the integral is split into a convergent quantity $f(r)$ (which contains the correlations) and a divergent constant Ω_ε (which is *independent* of r). Now that the integral has been split in this way, the integration is performed to give

$$(\gamma_q)_{0r;\varepsilon} = \Omega_\varepsilon - f(r) + O(\varepsilon^2 r^2) \quad (40)$$

with spatial correlators defined

$$f(r) \equiv \frac{1}{\pi\sqrt{2\tilde{K}}} \sum_{s=1}^r \left[\frac{1}{s - \frac{1}{2}} \right] \quad (41)$$

and the constant (divergent in ε) defined

$$\Omega_\varepsilon \equiv \frac{1}{2\pi\sqrt{2\tilde{K}}} \log\left(\cot\left(\frac{\varepsilon}{4}\right)\right). \quad (42)$$

With the regularized expression for correlators, quantities such as the *difference between correlators* are seen to remain finite in the limit of ε taken to zero and may easily be calculated

$$\lim_{\varepsilon \rightarrow 0} \left((\gamma_q)_{0r;\varepsilon} - (\gamma_q)_{0r';\varepsilon} \right) = f(r') - f(r). \quad (43)$$

Similarly it can be shown that, although the entanglement entropy of any block of L modes diverges in the massless case, the *difference* in entropy between two blocks is also convergent in the limit as ε is taken to zero. Thus, for instance, we may still make sense of how the entropy scaling of the state changes along the RG flow, as is done Fig. (6). The numeric RG of the critical ground-state, as undertaken in this work, was performed by choosing $\varepsilon \ll 1/R$ in (42), when working up to a maximum length scale of R modes, then using Eqns. (37), (40) for the ground-state covariances, ignoring the (small) $O(\varepsilon^2 R^2)$ corrections. For instance, working up to $R \approx 2000$ modes, we typically choose $\varepsilon \approx 1 \times 10^{-10}$ which is equivalent to setting $\Omega_\varepsilon \approx 4$ in (42).

[1] M.E. Fisher, Rev. Mod. Phys. **70**, 653 (1998).
[2] D.V. Shirkov, hep-th/9909024
[3] B. Delamotte, Am. J. Phys., **72**, 170184, (2004).
[4] L. P. Kadanov, Physics **2**, 263 (1966).

[5] K.G. Wilson, Rev. Mod. Phys. **47**, 4, 773.
[6] S. R. White, Phys. Rev. Lett. **69**, 2863 (1992), Phys. Rev. B **48**, 10345 (1993).
[7] U. Schollwoeck, Rev. Mod. Phys. **77**, 259 (2005),

- cond-mat/0409292.
- [8] G. Vidal, Phys. Rev. Lett. 99, 220405 (2007).
- [9] G. Vidal, quant-ph/0610099.
- [10] G. Evenbly, G. Vidal, arXiv:0710.0692v2 [quant-ph]
- [11] C. M. Dawson, J. Eisert, T. J. Osborne, arXiv:0705.3456v1.
- [12] M. Rizzi et al, arXiv:0706.0868.
- [13] G. Vidal, arXiv:0707.1454.
- [14] L. Cincio, J. Dziarmaga and M. M. Rams, arXiv:0710.3829.
- [15] M. Cramer et al, Phys. Rev. A **73**, 012309 (2006).